Reprinted from Journal of the Optical Society of America A

Modal characteristics of three-layered optical fiber waveguides: a modified approach

Charles Y. H. Tsao, David N. Payne, and W. Alec Gambling

Optical Fiber Group, Department of Electronics and Computer Science, University of Southampton, Southampton SO9 5NH, Hampshire, UK

Received May 23, 1988; accepted December 22, 1988

By invoking Debye potentials, we formulate exact eigenvalue equations and the corresponding field distributions for general, three-layered, radially stratified, dielectric, and nonferromagnetic metal, optical fibers. By using cross products of Bessel functions, which may be regarded as the basic functional elements of the eigenvalue equations, a comparison is made between the properties of a three-layer structure and a simple step-index profile, and a simple graphical solution is obtained. The technique is applied to several practical structures, including two-layer fibers having a central index depression in the core, ring-core fibers, W fibers, and progressively stepped three-layered structures. The mathematical procedure is simple, and the results are of interest to optical fiber designers.

1. INTRODUCTION

An optical fiber consisting of a core and surrounding cladding may be modeled conveniently by a single step-index profile, from which the modal propagation characteristics, dispersion properties, and power flow distributions can easily be described. In the continual search for a better fiber design, the multilayered structure has become increasingly popular.[1-18] To analyze this structure the simple step model should be replaced by a more appropriate multistep model, known as the radially stratified model.[3]

In addition to precise multilayered models, there are several well-developed approximations. These include the equivalent-step-index model and its improved version, known as the moment-equivalence model[4,15]; mode coupling between a core and claddings[5]; the index integral over the innermost layers[18]; and a variety of numerical approximations based on the weak-guidance assumption.[1,4,6-13] Although approximate analyses have obvious advantages, they have limitations and can cause errors if they are not used wisely.

The objective of this paper is to develop an *ad hoc* three-layered analysis technique that is exact for all-dielectric and/or nonferromagnetic metallic optical fibers and by which the propagation characteristics may be found graphically as for the simple step profile. Although the three-layered structure (TLS) involves only two discrete index steps, an understanding of its behavior may well be useful for analyzing a waveguiding structure that has more steps.

In particular, by invoking the well-known Debye potentials, in this paper it is shown how the exact eigenvalue equation (EVE) may be formulated for various TE, TM, HE, and EH modes. A brief summary is included of the major attributes of the cross products of Bessel functions, which may be regarded as the basic functional elements of the so-formed EVE. The use of the cross product not only enables one to compare directly a TLS with a typical single-step profile (SSP) but also permits a quick graphical solution. It is, of course, important to apply theoretical modelings to practical fibers such as typical monomode fibers with a central dip, ring fibers, W fibers, and progressively stepped three-layer fibers. As a result, a better physical understanding of the waveguide mechanism in various structures is provided, and some new empirical formulas concerning mode cutoff and dispersive properties are obtained.

2. EIGENVALUE EQUATION AND FIELD DISTRIBUTION

Figure 1(a) shows the cross section of a typical three-layered stratified fiber (i.e., a TLS) that has a core of radius r_1 and surrounding dielectric claddings of dividing radius r_2. The refractive indices of the three regions are n_1, n_2, and n_3, respectively; Figs. 1(b)–1(e) illustrate some selected index profiles. The first step is to establish the electromagnetic fields and then to formulate an analytic EVE for this fiber waveguide.

Assume that an electromagnetic wave is propagating along the z axis in a cylindrical coordinate system with a time–distance factor $\exp[-j(\omega t - \beta z)]$. Here ω is the circular frequency of the light and β is the propagation constant, which becomes complex for leaky modes. From the Debye potentials $\hat{z}_0\Psi e^{j\beta z}$ and $\hat{z}_0\Phi e^{j\beta z}$, associated with electric and magnetic fields $\mathbf{E} = \mathbf{e}e^{j\beta z}$ and $\mathbf{H} = \mathbf{h}e^{j\beta z}$, time-harmonic fields in the above radially stratified waveguide are well known to be[19]

$$\mathbf{e} = (\partial\Psi/r\partial\phi - \beta\partial\Phi/\omega\epsilon\partial r)\hat{r}_0 + (-\partial\Psi/\partial r - \beta\partial\Phi/\omega\epsilon r\partial\phi)\hat{\phi}_0 - (k^2n^2 - \beta^2)\Phi\hat{z}_0/j\omega\epsilon, \quad (1)$$

$$\mathbf{h} = (\partial\Phi/r\partial\phi + \beta\partial\Psi/\omega\mu\partial r)\hat{r}_0 + (-\partial\Phi/\partial r + \beta\partial\Psi/\omega\mu r\partial\phi)\hat{\phi}_0 + (k^2n^2 - \beta^2)\Psi\hat{z}_0/j\omega\mu. \quad (2)$$

Here $\hat{r}_0$, $\hat{\phi}_0$, and $\hat{z}_0$ are the unit radial, tangential, and axial vectors, respectively; μ and ϵ are the magnetic permeability and the electric permittivity, which are region dependent.

Formidable as Eqs. (1) and (2) may look at first sight, they offer a straightforward way of depicting the fields for numerous modes, because Debye potentials satisfy the following Helmholtz equations[19]:

0740-3232/89/040555-09$02.00

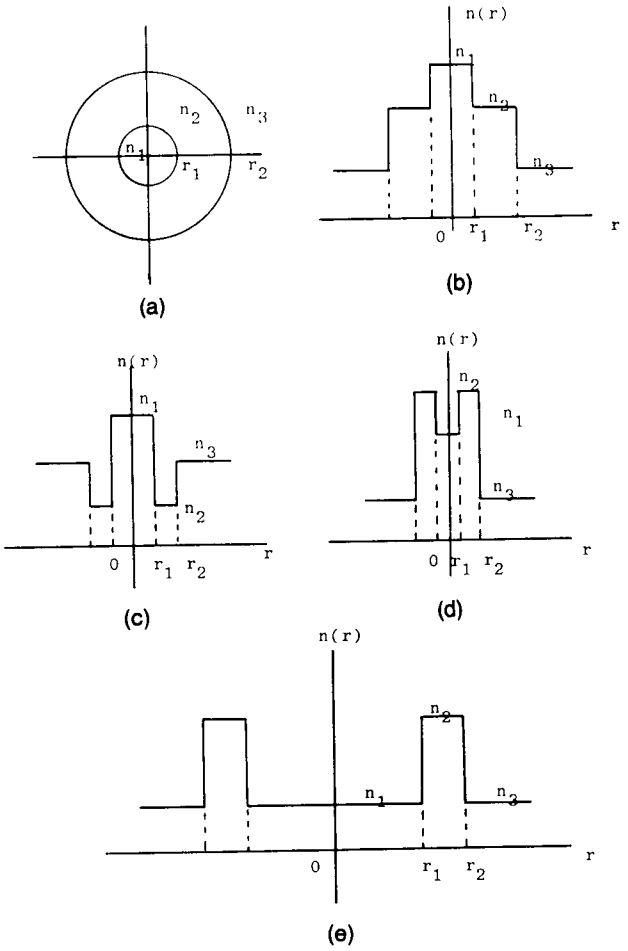

Fig. 1. Fiber cross section and index profiles for a three-layered radially stratified structure. (a) Cross section, (b) stepped three-layer fiber, (c) W fiber, (d) fiber with a central index dip, and (e) ring-core fiber.

$$[\Delta_t + (k^2 n_i^2 - \beta^2)]\Psi_i = 0 \tag{3}$$

and

$$[\Delta_t + (k^2 n_i^2 - \beta^2)]\Phi_i = 0 \tag{4}$$

(with the subscript i denoting the layer), of which the solution is already known. After Ψ and Φ are obtained, simple substitution into Eqs. (1) and (2) can be used to derive all the field components and therefore the EVE. This approach requires no special mathematical skills, but the formalism remains accurate and sufficiently concise. The TE mode is taken as an example to show how this is done.

By introducing $f_\nu(\phi) = e^{j\nu\phi}$ (ν is an integer), $U_1^2 = r_1^2(k^2 n_1^2 - \beta^2)$, $U_2^2 = r_1^2(k^2 n_2^2 - \beta^2)$, and $W_3^2 = r_2^2(\beta^2 - k^2 n_3^2)$, we find that the Ψ_i's are

$$\Psi_1 = A_1 J_\nu(U_1 r/r_1) f_\nu(\nu\phi), \tag{5a}$$

$$\Psi_2 = \{A_2 J_\nu(U_2 r/r_1) + B_2 Y_\nu(U_2 r/r_1)\} f_\nu(\nu\phi), \tag{5b}$$

$$\Psi_3 = A_3 K_\nu(W_3 r/r_2) f_\nu(\nu\phi), \tag{5c}$$

where J_ν, Y_ν, and K_ν are Bessel functions, Neumann (or Weber) functions, and modified Bessel functions of the second kind, respectively; and U_1, U_2, and W_3 are the layer phase parameters. For a TE mode, $\Phi_i = 0$ may be assumed, which, together with Eqs. (1), (2), and (5), gives the following transverse electric and axial magnetic field components:

$$e_{\phi 1} = -A_1(U_1/r_1) J_\nu'(U_1 r/r_1), \tag{6a}$$

$$e_{\phi 2} = -(U_2/r_1)[A_2 J_\nu'(U_2 r/r_1) + B_2 Y_\nu'(U_2 r/r_1)], \tag{6b}$$

$$e_{\phi 3} = -A_3(W_3/r_2) K_\nu'(W_3 r/r_2), \tag{6c}$$

$$h_{z1} = -(U_1^2/r_1^2 j\omega\mu) A_1 J_\nu(U_1 r/r_1), \tag{6d}$$

$$h_{z2} = -(U_2^2/r_1^2 j\omega\mu)[A_2 J_\nu(U_2 r/r_1) + B_2 Y_\nu(U_2 r/r_1)], \tag{6e}$$

$$h_{z3} = (W_3^2/r_2^2 j\omega\mu) A_3 K_\nu(W_3 r/r_2). \tag{6f}$$

The four coefficients A_1, A_2, A_3, and B_2 are chosen here to weight the field, but they are interdependent. They may be eliminated to produce the EVE, by applying boundary conditions such as those involving e_ϕ and h_z. For the structure depicted in Fig. 1 there are only two boundaries dividing the core and the inner and outer claddings; application of the continuity condition yields a 4×4 matrix whose determinant must be zero. Thus we have the following equations.

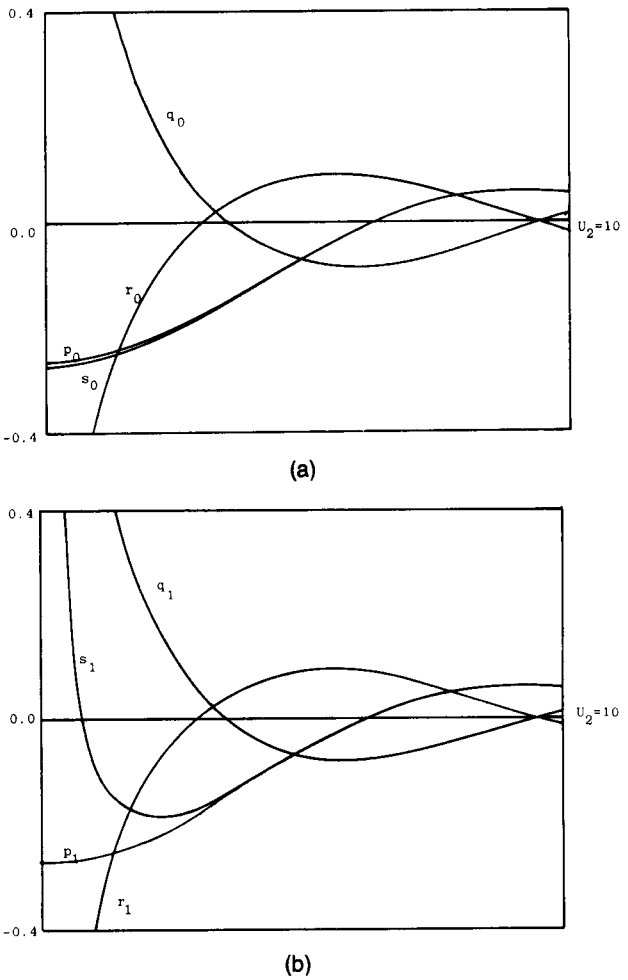

Fig. 2. Cross products of Bessel functions p_ν, q_ν, r_ν, and s_ν ($a = 1.5$) for (a) $\nu = 0$ and (b) $\nu = 1$.

TE Mode

$$J(r_\nu/aU_2 + Kp_\nu) = (Kq_\nu/U_2 + s_\nu/aU_2^2). \quad (7)$$

Here $a = r_2/r_1$ is the ratio of the two radii, $J = J_\nu'(U_1)/U_1J_\nu(U_1)$ and $K = K_\nu'(W_3)/W_3K_\nu(W_3)$; and $p_\nu = J_\nu(aU_2)Y_\nu(U_2) - J_\nu(U_2)Y_2(aU_2)$, $q_\nu = J_\nu(aU_2)Y_\nu'(U_2) - J_\nu'(U_2)Y_\nu(aU_2)$, $r_\nu = J_\nu'(aU_2)Y_\nu(U_2) - J_\nu(U_2)Y_\nu'(aU_2)$, and $s_\nu = J_\nu'(aU_2)Y_\nu'(U_2) - J_\nu'(U_2)Y_\nu'(aU_2)$ are the cross products of Bessel and Neumann functions.[20,21] These Bessel products were studied thoroughly in Refs. 20 and 21. Their basic features are plotted in Figs. 2, and some asymptotic approximations are listed in Appendix A.

This routine is repeatable for the TM mode ($\Psi_i = 0$) and the hybrid mode ($\Phi \neq 0$, $\Psi \neq 0$), and the final EVE's take the form of Eqs. (8) and (9).

TM Mode

$$J(s_{23}r_\nu/aU_2 + Kp_\nu) = s_{21}(Kq_\nu/U_2 + s_{23}s_\nu/aU_2^2). \quad (8)$$

HE or EH Mode

$$\begin{aligned} p_\nu^2 &+ 2x_1x_2(n_2^2/n_1n_3)(2/\pi aU_2^2)^2 \\ &+ x_1^2x_2^2[J(r_\nu/aU_2 + Kp_\nu) - (Kq_\nu/U_2 + s_\nu/aU_2^2)] \\ &\times [J(s_{23}r_\nu/aU_2 + Kp_\nu) - s_{21}(Kq_\nu/U_2 + s_{23}s_\nu/aU_2^2)] \\ &= x_1^2(Jp_\nu - s_{21}q_\nu/U_2)(Jp_\nu - q_\nu/U_2) \\ &+ x_2^2(Kp_\nu + s_{23}r_\nu/aU_2)(Kp_\nu + s_{23}r_\nu/aU_2). \end{aligned} \quad (9)$$

Here $s_{21} = n_2^2/n_1^2$, $s_{23} = n_2^2/n_3^2$, $x_1^2 = k^2n_1^2U_1^4U_2^4/\nu^2\beta^2V_{12}^4$, $x_2^2 = k^2n_3^2a^4U_2^4W_3^4/\nu^2\beta^2V_{23}^4$, $V_{12}^2 = k^2r_1^2(n_1^2 - n_2^2)$, and $V_{23}^2 = k^2r_2^2(n_2^2 - n_3^2)$; and k represents the free-space wave number. In the weak-guidance limit, $s_{21} \approx 1$ and $s_{23} \approx 1$ may be assumed in Eqs. (7)–(9), and the first term p_ν^2 in Eq. (9) may virtually be neglected. In general, however, the EVE's expressed in Eqs. (7)–(9) must be considered, since they are exact for all kinds of all-dielectric and metallic fibers.

3. GRAPHICAL SOLUTION OF THE EIGENVALUE EQUATION

As with the EVE of the SSP, the EVE of the TLS can be solved graphically. The graphical method offers an alternative approach to determining the solutions of transcendental equations such as Eqs. (7)–(9). Equation (7) is taken as an example to show why this is possible and how it can be done.

In order for the graphical method to be viable, all functions appearing in Eq. (7) must be real and capable of being plotted as a function of a single variable such as U_1, U_2, or the equivalent index $n_e = \beta/k$. It is convenient, for example, to plot $J(r_\nu/aU_2 + Kp_\nu)$ as the left-hand curve and $Kq_\nu/aU_2 + s_\nu/aU_2^2$ as the right-hand curve on the same diagram (see Fig. 3). The crossings of these curves correspond to the solutions: a single crossing represents a single TE ν mode, and the absence of a crossing indicates a cutoff.

Some care is required with this simple graphical method because the U parameter may become purely imaginary whenever n_e exceeds n_1 or n_2. Should this be the case, the U parameter must be replaced by the relevant W parameter, namely, $U = jW$. Two distinct cases are now examined individually.

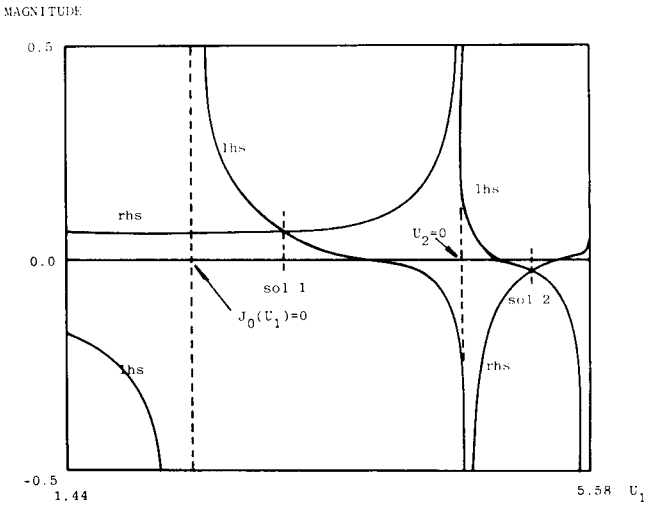

Fig. 3. Graphical method of solving Eq. (7): $n_1 = 1.47$, $n_2 = 1.462$, $n_3 = 1.458$, $r_1 = 3.0\ \mu m$, $r_2 = 5.0\ \mu m$, and $\nu = 0$. rhs, Right-hand side; lhs, left-hand side; sol 1 and sol 2, solutions for cases 1 and 2, respectively.

Case 1: $n_e > n_1$

Case 1 is that of a fiber having a central index dip or that of a ring-core fiber [Figs. 1(d) and 1(e)]. In this case, $U_1 = jW_1$ and $W_1^2 = k^2r_1^2(n_e^2 - n_1^2)$, giving $J = J_\nu'(jW_1)/jW_1J_\nu(jW_1) = -I_\nu(W_1)/W_1I_\nu(W_1)$ (I_ν is the modified Bessel function of the first kind), which is real. Since K and all cross products remain real, Eq. (7) is still defined in terms of real-valued functions, which is amenable to the graphical method.

Case 2: $n_e > n_2$

Case 2 represents a matched or depressed W-fiber profile, for which $U_2 = jW_2$ and $W_2^2 = k^2r_1^2(n_e^2 - n_2^2)$. It follows that $p_\nu = -(2/\pi)[I_\nu(aW_2)K_\nu(W_2) - I_\nu(W_2)K_\nu(aW_2)]$, $q_\nu/U_2 = (2/\pi W_2)[I_\nu(aW_2)K_\nu'(W_2) - I_\nu'(W_2)K_\nu(aW_2)]$, $r_\nu/aU_2 = (2/\pi aW_2)[I_\nu'(aW_2)K_\nu(W_2) - I_\nu(W_2)K_\nu'(aW_2)]$, and $s_\nu/aU_2^2 = -(2/\pi aW_2^2)[I_\nu'(aW_2)K_\nu'(W_2) - I_\nu'(W_2)K_\nu'(aW_2)]$, in view of $J_\nu(jW_2) = \exp(j\nu\pi/2)I_\nu(W_2)$ and $Y_\nu(jW_2) = \exp[j(\nu + 1)\pi/2]I_\nu(W_2) - (2/\pi)\exp(-j\nu\pi/2)K_\nu(W_2)$ (see Appendix A). All these expressions, coupled with real values of J and K, make Eq. (7) a real function for which the graphical approach is possible.

The accuracy of the graphical solution depends on the scale of the drawing, of course. For most practical purposes, it may be sufficient to calculate 320 points for each frame in order to achieve an accuracy of 10^{-4} at the cost of a few seconds of computation time on an IBM personal computer.

4. THREE-LAYERED STRUCTURE AND SINGLE STEP PROFILE

The TLS comprises two single index steps (i.e., SSP's); it can also reduce to a two-layered structure. In this case Eqs. (7)–(9) can be reworked to yield the EVE's of single-step waveguides. Here the TE mode is taken as an example to explain how the exact EVE's summarized in this paper can be reduced easily to ordinary two-layer ones.

$r_2 \to \infty$, or $r_2/r_1 \to \infty$

When the inner cladding is thick enough, the TLS obviously reduces to the SSP with core and cladding indices n_1 and n_2,

respectively, and a core radius r_1. The condition $a \to \infty$ implies that $r_\nu/aU^2 \ll Kp_\nu$, $s_\nu/aU_2^2 \ll Kq_\nu$, and $q_\nu/U_2p_\nu \approx -K'(W_2)/W_2K(W_2)$ (see Appendix A), and ultimately Eq. (7) becomes

$$J_\nu'(U_1)/U_1J_\nu(U_1) = -K'(W_2)/W_2K(W_2), \tag{7a}$$

which is the TE-mode EVE of the specified SSP.[22]

$r_2 \to r_1$, or $r_2/r_1 \to 1 + d (d \to 0)$

The relation $r_2 \to r_1$ depicts an SSP with core and cladding indices n_1 and n_3 and a core radius r_1. It can easily be shown that $p_\nu = -(2/\pi)d \to 0$, $q_\nu = 2/\pi U_2$, $r_\nu = -2/\pi aU_2$, and $s_\nu = (2d/\pi)(\nu^2/U_2^2 - 1) \to 0$ for $a \to 1$ (see Appendix A), indicating that

$$J_\nu'(U_1)/U_1J_\nu(U_1) = -K_\nu'/W_3K_\nu(W_3) \tag{7b}$$

for Eq. (7), as is expected.[22]

$n_1 = n_2$

The TLS with $n_1 = n_2$ is the SSP fiber with a core radius r_2. For such a profile, $V_{12}^2 = 0$, and so $U_1 = U_2$, $J_\nu'(U_1)/U_1J_\nu(U_1) = J_\nu'(U_2)/U_2J_\nu(U_2)$. Substitution into Eq. (7) gives

$$K = -(1/aU_2)[r_\nu - s_\nu J_\nu(U_2)/J_\nu'(U_2)]/[p_\nu - q_\nu J_\nu(U_2)/J_\nu'(U_2)],$$

or, more precisely, after a little straightforward algebra,

$$K_\nu'(W_3)/W_3K_\nu(W_3) = -J_\nu'(aU_2)/aU_2J_\nu(aU_2). \tag{7c}$$

This is the TE-mode EVE for the SSP of radius r_2.[22]

$n_2 = n_3$

The TLS is once again reduced to an SSP but with a core radius r_1. It would now be more convenient to refer to $U_2 = jW_2$, and $aW_2 = W_3$ in view of $V_{23}^2 = 0$. Proceeding as above, we may first rewrite Eq. (7) as

$$J = (q_\nu/U_2 + s_\nu/KaU_2)/(p_\nu + r_\nu/KaU_2)$$

and then obtain straightaway the SSP TE-mode EVE,[22]

$$J_\nu'(U_1)/U_1J_\nu(U_1) = -K_\nu'(W_2)/W_2K_\nu(W_2). \tag{7d}$$

5. THREE-LAYERED STRUCTURE OF A TYPICAL MONOMODE FIBER WITH A CENTRAL INDEX DIP

The index profile of a typical monomode fiber often has a central dip in the core and many random ripples in the cladding as shown in Fig. 4(a).[4] As far as the modeling is concerned, it is a common practice to smooth out those ripples. The existence of a central dip, as the TLS analysis tends to suggest, may not be important if it is sufficiently narrow. This is verified by numerous experimental observations, but one may ask, How wide may the dip be before it affects noticeably the modal characteristics?

Two important cases are investigated: a deep dip and a shallow dip. In either case it is found that $1/a^2 \ll 1$ is the only precondition that limits the effects of the central dip regardless of its actual index. In other words, since $r_2 \approx (3\text{–}5)\lambda$ (λ is the wavelength) is true for most monomode fibers, the radius of its central dip must satisfy $r_1 < \lambda$.

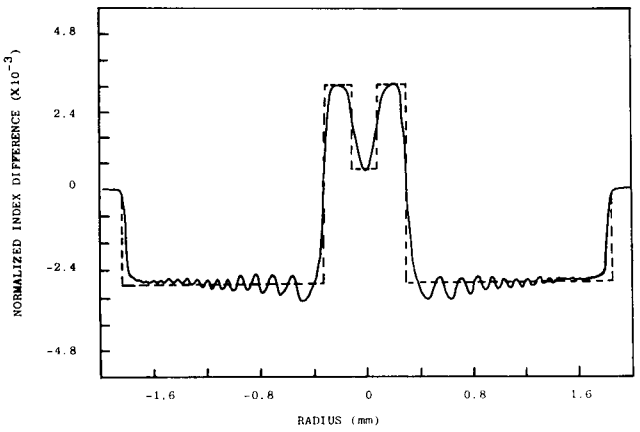

(a)

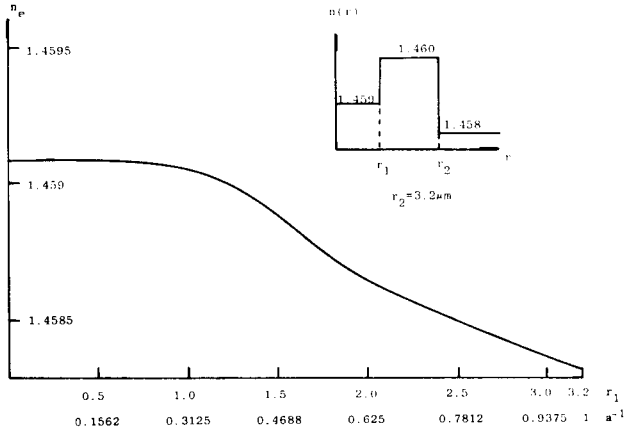

(b)

Fig. 4. (a) Measured refractive-index profile, showing a central index dip; (b) equivalent index n_e of the fundamental mode as a function of the radius of the index dip.

$(n_2 - n_3) \ll (n_2 - n_1)$ and $r_1 \ll r_2$

As $r_1 \to 0$, $U_2 \to 0$ and $W_1 \to 0$; accordingly $J_\nu'(U_1)/U_1J_\nu(U_1) = -I_\nu'(W_1)/W_1I_\nu(W_1) \ll 1$. Now Eq. (7) may be rearranged as (for $\nu \geq 1$)

$$-K_\nu'(W_3)/W_3K_\nu(W_3) = [J_\nu'(aU_2)/aU_2J_\nu(aU_2)] \times (1 - a^{-2\nu+1})/(1 + a^{-2\nu}). \tag{10}$$

The condition that $a^{-2\nu} \ll 1$ makes Eq. (10) practically identical to Eq. (7c), which is the EVE without the dip.

$(n_2 - n_1) \ll (n_2 - n_3)$ and $r_1 \ll r_2$

Since $r_1 \to 0$ and $n_1 > n_3$, it is possible to observe a real U_1 although it is small. $U_1 \to 0$ implies that $J_\nu'(U_1)/U_1J_\nu(U_1) \to \infty$ (for $\nu \geq 1$), which, in association with $U_2 \to 0$, would change Eq. (7) to

$$-K_\nu'(W_3)/W_3K_\nu(W_3) = [J_\nu'(aU_2)/aU_2J_\nu(aU_2)] \times (1 + a^{-2\nu})/(1 - a^{-2\nu}). \tag{11}$$

Like Eq. (10), Eq. (11) may be treated as Eq. (7c) under the condition that $a^{-2\nu} \ll 1$.

Figure 4(b) demonstrates how n_e of the fundamental mode varies as the dip widens from 0 to r_2 as computed from Eq.

(9). It is evident that n_e is not affected while $a^{-2} \ll 1$; this result agrees quite well with the above analyses.

6. RING FIBER WAVEGUIDE

The ring fiber waveguide (RFW) is a waveguide in which the high-index core is in the form of a thin-walled tube, with inner and outer lower-index claddings; it is sometimes referred to as the tubular or annular waveguide. This tubular fiber waveguide, which has a typical diameter of (50–100)λ, can produce single or multiple images of one endface on the opposite one; and this "self-imaging" may permit applications as monomode fiber-optic 3 dB-directional couplers.[14]

Self-Imaging and Interference

Figure 5 schematically illustrates how the self-imaging effects are obtained. The TEM_{00} radiation from a tunable dye laser is focused as a diffraction-limited spot onto a point (e.g., $\phi = 0$) on the input end face of the core. By means of Fourier–Fresnel representation,[14] this input radiation may be decomposed into a superposition of numerous TE_ν modes; ν ranges from 0 to an arbitrarily large integer. With no loss of generality, let us plot two lower-order modes ($\nu = 1$, 2) against a ϕ axis, describing a single light spot at $\phi = 0$ [Fig. 6(a)]. Because of the phase difference of the two modes, they will interfere with each other as they propagate down the tubular fiber. It is evident that, when the phase difference is $\pi/2$ or π, two separate light spots at $\phi = 0, \pm\pi$ or a single inverted light spot at $\phi = \pi$ is produced [Figs. 6(b) and 6(c)]. For the ring core fibers reported in Ref. 14, of which $n_1 = n_3 = 1.458$, $n_2 = 1.462$, $r_1 \approx r_2 \approx 32.5\ \mu m$, $r_2 - r_1 \approx 2\ \mu m$, and $\lambda = 0.59\ \mu m$, the interference length is calculated to be 110 mm according to Eq. (7), a value that agrees reasonably well with the measured experimental result (101 mm).

Diameter of the Ring Fiber Waveguide

It must be stressed that, for satisfactory self-imaging effects to be achieved, the tubular core must be sufficiently large in diameter and sufficiently thin, as both experiment and theory suggest. A fiber having a small tubular core is no differ-

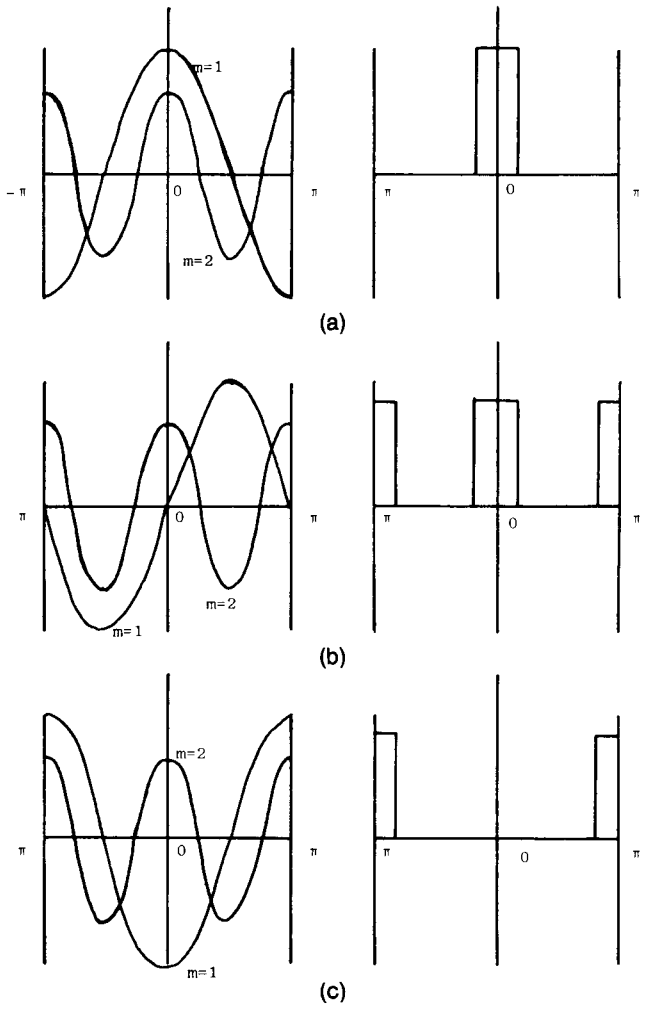

Fig. 6. Light spots as a function of ϕ are superposed to include sin ϕ and sin 2ϕ: (a) sin ϕ and sin 2ϕ at the input end face, (b) $\pi/2$ phase shift in sin ϕ over $L/2$, and (c) π phase shift in sin ϕ at L.

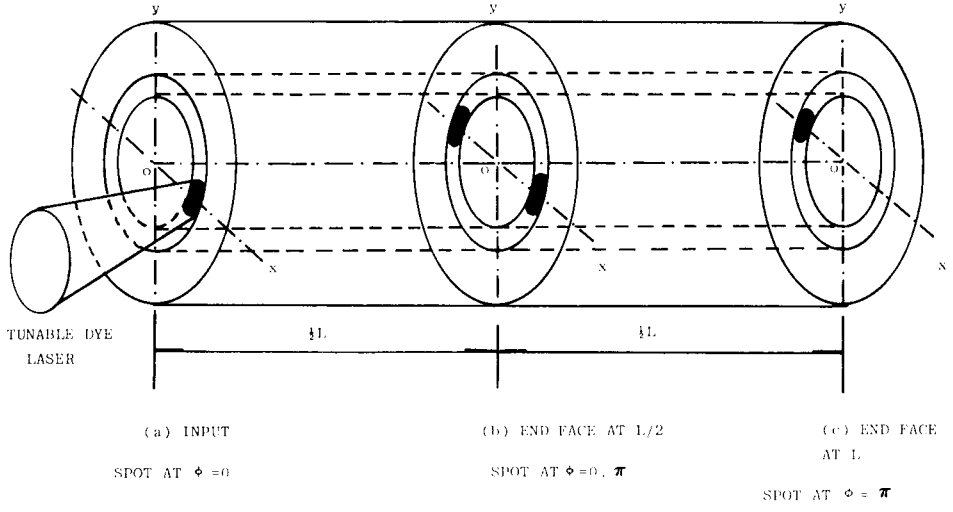

Fig. 5. Self-imaging effects in a ring-core fiber with (a) a single light spot at the input end face, (b) two light spots at the end face after a half interference length $L/2$, and (c) an inverted light spot at the end face after the interference length L.

ent from an ordinary monomode fiber having a moderate central index dip, which cannot support many modes as required by the Fourier–Fresnel expansion. Our analyses show that $r_1 > 50\lambda$ or more is necessary to permit sufficient modes for self-imaging to be produced, a result that agrees well with experiments.

Thickness of the Ring Core

In order for the RFW to be treated as a wrapped-up single-mode slab waveguide, its wall should not be thick. The mathematical translation of this thin-wall requirement is to have a single ν-mode operation in a RFW, implying the existence of a unique, single mode for a selected integer ν. This is possible only for the RFW, and we shall establish it by using the graphics method introduced in Section 3.

Note that $r_1 \approx r_2 \gg (r_2 - r_1)$ and $n_1 = n_3$ and therefore that $W_1 \gg 1$, $U_2 \gg 1$, $J \approx K$, $r_\nu \approx -q_\nu$, and $s_\nu \approx p_\nu$ must apply in a RFW. When these relations are combined Eq. (7) is then simplified to

$$K[(a+1)/aU_2]q_\nu = (K^2 - 1/aU_2^2)p_\nu. \tag{12}$$

Here p_ν and q_ν may be approximated accurately by their asymptotic formulas (refer to Appendix A) so that

$$p_\nu \approx -[2/\pi(aU_2)^{1/2}]\sin(a-1)U_2,$$

$$q_\nu \approx [2/\pi(aU_2)^{1/2}]\cos(a-1)U_2.$$

It is obvious that the condition $V_{23} < \pi/(a-1)$ is necessary in order for a single crossing to be obtained between the right-hand and left-hand sides of Eq. (12) (see Fig. 7). Introducing a new parameter $V_r = k(r_2 - r_1)(n_2^2 - n_3^2)^{1/2}$, which is more convenient in this case, we deduce $V_r < \pi$ to be the single ν-mode operation condition for a RFW. This formula has slightly relaxed the condition that $V < 2.405$, the single-mode condition for an ordinary SSP.

7. W-FIBER WAVEGUIDE

The W fiber [Fig. 1(c)] represents another large class of promising monomode fibers because it possesses a bigger core, a better field confinement (and therefore less vulnerability to bending loss), and, best of all, desirable dispersive properties.[1,2] Our analysis shows that any practical W fiber can be modeled by the n_1/n_2 SSP, formed between the core and the inner cladding, plus an additional mode supressor to cut off or, more precisely, to leak away any modes of which the equivalent refractive index is below the outer cladding index n_3. The validity of this remarkably simple yet accurate model hinges on a single criterion, i.e., $(r_2 - r_1)/r_1 > 0.17$, that is met automatically by almost all monomode fiber designs. The question of how fast the higher-order modes are attenuated away by the outer cladding is not discussed here, but, within the objective of this paper, it is sufficient to note that a smaller r_2 produces a higher attenuation and, under most practical circumstances, a micrometer increment in r_2 may make a significant difference.

A W fiber can be treated as a form of TLS. Its waveguide parameter lies between those of two SSP's: the inner step (IS) (n_1/n_2 SSP) or the outer step (OS) (n_1/n_3 SSP). The SSP that most closely resembles the W fiber depends entirely on the thickness of the inner cladding because, when $(r_2 - r_1)/r_1 \to 0$ or ∞, the TLS reduces to the OS or the IS, respectively.

Now define $V_{13} = kr_1(n_1^2 - n_3^2)^{1/2}$ ($V_{12} > V_{13}$) and mark it and U_1^{13} ($HE_{11}U$ value of the OS) on the Y axis at $X = (r_2 - r_1)/r_1 = 0$ (Fig. 8). For $X = \infty$ similar points may be marked for the IS. Because $V_{12} > V_{13}$ (because $n_2 < n_3$ for a W fiber), $U_1^{12} > U_1^{13}$. When r_2 lies between r_1 and ∞, its U_1 value must lie between U_1^{13} and U_1^{12}. The exact results are, of course, calculable from Eqs. (7)–(9), and they are plotted in Fig. 8 for some common monomode W-fiber designs. The condition that $(r_2 - r_1) > \lambda$, or $(r_2 - r_1)/r_1 > 0.17$, is sufficient to ensure that $U_1 = U_1^{12}$, almost irrespective of the index n_2. On the other hand, U_1 becomes approximately equal[13] to U_1 only for extremely small $(r_2 - r_1)$, namely, $(r_2 - r_1) < 0.01\lambda$, or $(r_2 - r_1)/r_1 < 0.0017$, which is interesting. It must be noted that the core usually is shielded completely by a relatively thick lower-index cladding in most designs in order to take full advantage of a W fiber. In other words, $(r_2 - r_1) > \lambda$ is usually true, so the U parameters, together with the modal propagation constants, are determined by the IS SSP. This fact simplifies the W-fiber cutoff analyses tremendously: a mode experiences cutoff as soon as its U value of the IS

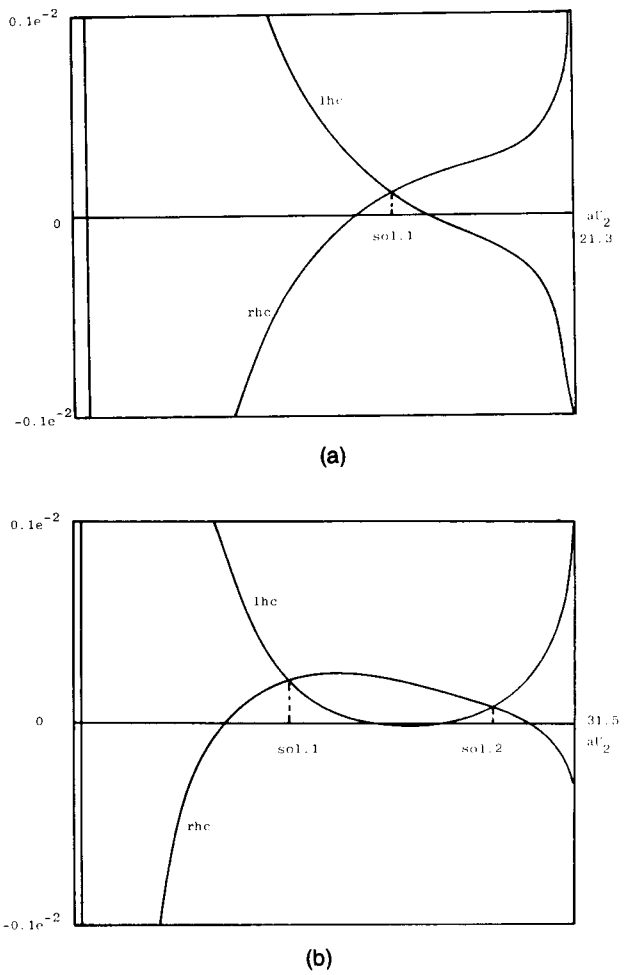

Fig. 7. Number of ν modes m are determined by $(m-1)\pi < V_r < m\pi$. (a) Single-ν-mode operation ($m = 1$) for $n_1 = n_3 = 1.458$, $n_2 = 1.461$, $r_1 = 20\ \mu m$, $r_2 = 23\ \mu m$; (b) double-ν-mode operation ($m = 2$) for $n_1 = n_3 = 1.458$, $n_2 = 1.464$, $r_1 = 20\ \mu m$, $r_2 = 24\ \mu m$. rhc, Right-hand core; lhc, left-hand core.

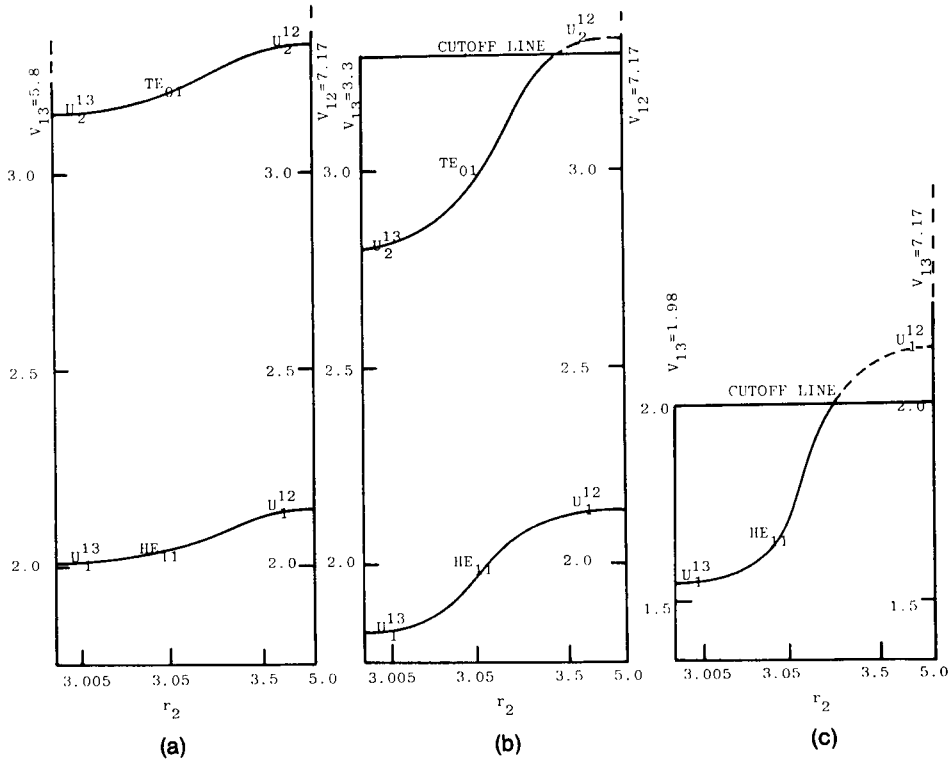

Fig. 8. The parameter U as a function of r_2 in a W fiber for which $n_1 = 1.46$, $n_2 = 1.44$, and $r_1 = 3.0\ \mu m$: (a) $n_3 = 1.45$, no cutoff for HE_{11}–TE_{01} mode; (b) $n_3 = 1.4558$, TE_{01}-mode cutoff; (c) $n_3 = 1.4585$, both TE_{01}- and HE_{11}-mode cutoffs.

exceeds V_{13}. However $U > V_{13}$ means simply that $n_e < n_3$, and the cutoff results are well anticipated.

Bearing this in mind, one may quickly predict a fundamental mode cutoff if the U parameter evaluated for the core–inner-cladding step is greater than V_{13}; and monomode operation is possible if the TE_{01}-mode U value is greater than V_{13} (Fig. 8). It can be seen that it is not the condition $V_{13} < 2.405$, but $V_{13} < U^{12}$ of TE_{01}, that leads to monomode operation of a W fiber, which can be at a wavelength as much as 50% larger than for any ordinary SSP.[1,2] This is the key factor to all desired waveguide characteristics.

8. STEPPED THREE-LAYER STRUCTURE

Surprisingly, perhaps, the stepped TLS (STL) [Fig. 1(b)] appears to be more difficult to analyze precisely than does the W-fiber waveguide. This is due to the wide range of waveguide characteristics that are possible, as may become clear from the following examples. As a simple but useful approximation, a STL may be treated as the SSP formed between n_1 and n_2, plus a high-order mode adder. To be more precise, we can state this equivalence as follows: if $n_1 > n_e > n_2$, then the n_e is determined by the n_1/n_2 SSP. On the other hand, if $n_e < n_2$, then the n_e is mainly characteristic of the SSP formed between n_2 and n_3, as is discussed below.

Effects of n_2

The behavior of a STL is strongly dependent on n_2, particularly when n_2 is close to n_1 and $(r_2 - r_1) > \lambda$, as is expected intuitively. A typical n_2 dependence of the equivalent index n_e is given in Fig. 9(a) for the TE_{01} mode of a fiber having typical practical values of n_1 and n_3; here every parameter is fixed except n_2, which varies from n_3 to n_1. It is clearly seen that, when $(r_2 - r_1) < \lambda$, this relation is nearly linear, which may provide some ground for a perturbation approximation or a linear interpolation. The dependence does, however, become highly nonlinear for $(r_2 - r_1) \gg \lambda$: n_e becomes saturated for $n_2 \ll n_1$, signifying an n_1/n_2 SSP guidance, but rapidly approaches n_1 as $n_2 \to n_1$.

Effect of r_1

By maintaining all parameters constant except r_1, we may determine its effect on the equivalent index of the TE_{01} mode. A typical result is illustrated in Fig. 9(b). Not surprisingly, n_e decreases as r_1 decreases, indicating that the light is guided by the n_1/n_2 SSP, gradually to the point at which $n_e = n_2$. Below this point the majority of light is guided only by the n_2/n_3 step. As a result, further decreases in r_1 make n_e flatten out, as shown in Fig. 9(b). This phenomenon is particularly important for coupler design.

Effect of r_2

The radius r_2, like n_2, plays a vital part in determining the degree of modal adder that a STL exhibits. A typical r_2 dependence is demonstrated in Fig. 9(c), in which high-order TE_0 modes are also inserted. There is only one mode for which $n_1 > n_e > n_2$, namely, the TE_{01} mode for $n_2 = 1.461$, and its n_e is seen to be dominated by the n_1/n_2 SSP guidance mechanism. For all other added high-order modes, of which the number increases as r_2 increases, $n_e < n_2$, showing clearly the influence of the n_2/n_3 SSP.

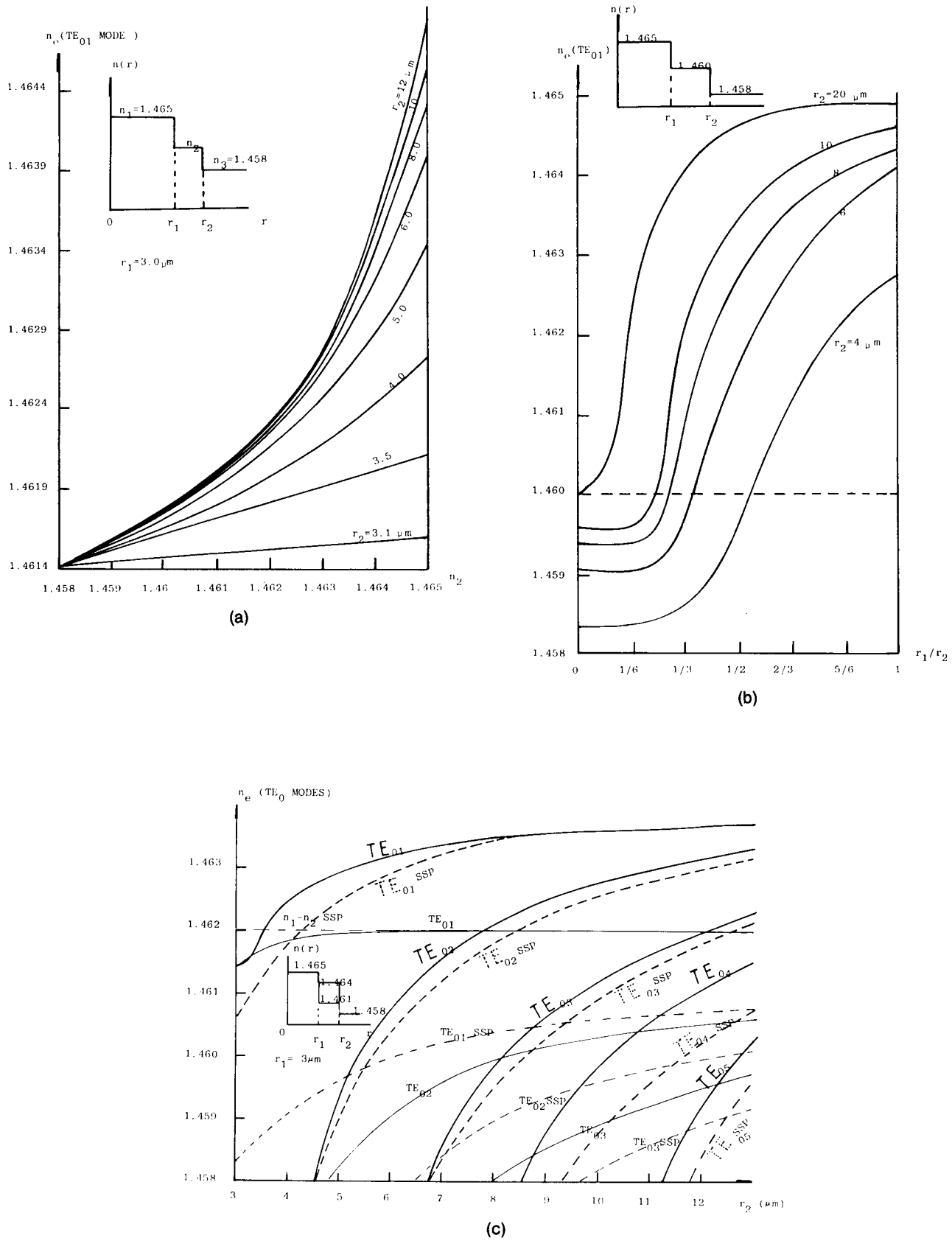

Fig. 9. Equivalent refractive indices as functions of the geometry and the index profile for a stepped three-layer fiber: (a) n_2 dependence, (b) r_1 dependence, and (c) r_2 dependence. In (c) the thick curves are for $n_2 = 1.464$, the thin curves are for $n_2 = 1.461$, and the dashed curves are for the n_2/n_3 SSP's.

9. CONCLUDING REMARKS

The exact EVE's have been formulated for a general three-layered, all-dielectric or nonferromagnetic metallic, fiber waveguide. The simple formalism presented here involves only the Bessel functions and their cross products. As a result, the EVE's can be solved graphically. The method can be applied easily to many practical waveguide structures, such as single-mode fibers showing a central index dip, large-diameter ring-core fibers, W fibers, and progressively stepped three-layer fibers.

APPENDIX A: p_ν, q_ν, r_ν, AND s_ν

1. The asymptotic formulas of p, q, r, and s when $a \to 1 + d$ $(d \to 0)$ are

$$p_\nu \approx (2/\pi)d,$$

$$q_\nu \approx 2/\pi U_2,$$

$$r_\nu \approx -2/\pi U_2,$$

$$s_\nu \approx (2d/\pi)(\nu^2/U_2^2 - 1).$$

2. The asymptotic formulas of p, q, r, and s for $U_2 \to \infty$ and U_2 real are

$$p_\nu = s_\nu = -(2/\pi U_2 a^{1/2})\sin(a-1)U_2,$$

$$q_\nu = -r_\nu = (2/\pi U_2 a^{1/2})\cos(a-1)U_2.$$

3. The alternative formulas of p, q, r, and s for $U_2 = jW_2$ are

$$p_\nu = -(2/\pi)[I_\nu(aW_2)K_\nu(W_2) - I_\nu(W_2)K_\nu(aW_2)]$$

$$q_\nu = j(2/\pi)[I_\nu(aW_2)K_\nu'(W_2) - I_\nu'(W_2)K_\nu(aW_2)],$$

$$r_\nu = j(2/\pi)[I_\nu'(aW_2)K_\nu(W_2) - I_\nu(W_2)K_\nu'(aW_2)],$$

$$s_\nu = (2/\pi)[I_\nu'(aW_2)K_\nu'(W_2) - I_\nu'(W_2)K_\nu'(aW_2)].$$

4. The asymptotic formulas of p, q, r, and s, when $U_2 = jW_2$, W_2 is real, and $W_2 \to \infty$ or $a \to \infty$, are

$$p_\nu = -(2/\pi)I_\nu(aW_2)K_\nu(W_2),$$

$$q_\nu = j(2/\pi)I_\nu(aW_2)K_\nu'(W_2),$$

$$r_\nu = j(2/\pi)I_\nu'(aW_2)K_\nu(W_2),$$

$$s_\nu = (2/\pi)I_\nu'(aW_2)K_\nu'(W_2).$$

ACKNOWLEDGMENTS

This study is sponsored by the Science and Engineering Research Council, UK, and its support is gratefully acknowledged. We thank Simon Poole and Peter Harris for provision of the fiber details described in Ref. 14. We also thank James J. Burke for his many invaluable comments and suggestions for the improvement of the manuscript during its preparation.

REFERENCES

1. S. Kawakami and S. Nishida, "Characteristics of a doubly clad optical fibre with a low-index inner cladding," IEEE J. Quantum Electron. **QE-10,** 879–887 (1974).
2. S. Kawakami, "Low dispersion/low loss single mode optical fibres—topics related with W-fibres," J. Inst. Electron. Commun. Eng. Jpn. (Japan) **68,** 860–865 (1985).
3. C. Yeh and G. Lindgren, "Computing the propagation characteristics of radially stratified fibers: an efficient method," Appl. Opt. **16,** 483–493 (1977).
4. P. L. François, M. J. Adams, R. J. Mansfield, R. D. Birch, and E. J. Tarbox, "Equivalent step-index profile for general W-fibres: application to TE_{01} mode cut-off," Opt. Quantum Electron. **14,** 483–499 (1982).
5. P. L. François and C. Vassallo, "Finite cladding effects in W fibers: a new interpretation of leaking modes," Appl. Opt. **22,** 3109–3120 (1983).
6. R. A. Sammut, "Range of monomode operation of W-fibres," Opt. Quantum Electron. **10,** 509–514 (1978).
7. M. Monerie, "Propagation in doubly clad single-mode fibers," IEEE J. Quantum Electron. **QE-18,** 535–542 (1982).
8. A. S. Belanov, E. M. Dianov, G. I. Ezhov, and A. M. Prokhorov, "Propagation of normal modes in multilayered optical waveguides. I. Component fields and dispersion characteristics," Sov. J. Quantum Electron. **6,** 43–50 (1976).
9. A. S. Belanov, E. M. Dianov, G. I. Ezhov, and A. M. Prokhorov, "Propagation of normal modes in multilayered optical waveguides. II. Energy characteristics," Sov. J. Quantum Electron. **6,** 915–920 (1976).
10. C. D. Hussey and F. De Fornel, "Effective refractive index and range of monomode operation for W-fibres," Electron. Lett. **20,** 346–347 (1984).
11. H. M. Barlow, "A cladded tubular glass-fibre guide for single-mode transmission," J. Phys. D **14,** 405–412 (1981).
12. H. M. Barlow, "A large diameter optical-fibre waveguide for exclusive transmission in the HE_{11} mode," J. Phys. D **16,** 1439–1451 (1983).
13. H. M. Barlow, "A new large-diameter optical fibre waveguide for operation in the TE_{01} mode," J. Phys. D **18,** 1511–1520 (1985).
14. Th. Niemeier, S. B. Poole, and R. Ulrich, "Self-imaging by ring-core fibers," in *Digest of Topical Meeting on Optical Fiber Communication*, I. D. Aggarwal, ed. (Optical Society of America, Washington, D.C., 1985), pp. 122–124.
15. R. J. Black, and C. Pask, "Equivalent optical waveguides," IEEE J. Lightwave Technol. **LT-2,** 268–276 (1984).
16. A. Majewski, "Numerical analysis of double-step-index single-mode optical fibres," Arch. Electrotech. **33,** 257–265 (1984).
17. M. Kuroda, "Transmission characteristics of polarization-maintaining optical fiber with three-layer elliptical cross-section," Trans. Inst. Electron. Commun. Eng. Jpn. B **68,** 93–100 (1985).
18. G. Coppa and P. Di Vita, "Cut-off condition of the fundamental mode in monomode fibres," Opt. Commun. **49,** 409–412 (1984).
19. W. R. Smythe and C. Yeh, "Formulas," in *American Institute of Physics Handbook*, 3rd ed., D. E. Gray, ed. (McGraw-Hill, New York, 1972), Sec. 5, pp. 5–45.
20. M. Abramowitz and I. A. Stegun, eds., *Handbook of Mathematical Functions* (Dover, New York, 1965), Chap. 9.
21. E. T. Goodwin, "Recurrence relations for cross-products of Bessel functions," Q. J. Mech. Appl. Math. **11,** 72–74 (1949).
22. M. J. Adams, *An Introduction to Optical Waveguides* (Wiley, Chichester, UK, 1981), p. 225.